Energy- and Angle-Resolved Fragmentation of Ethyl Bromide on GaAs(110)

Khalid A. Khan,* Joseph E. Moryl, David A. Slater, Peter J. Lasky, and Richard M. Osgood, Jr.

Columbia Radiation Laboratory, Columbia University, New York, New York 10027

Received: June 17, 1997; In Final Form: August 11, 1997[⊗]

Angle- and mass-resolved time-of-flight (TOF) measurements are used to probe the photodynamics and molecular orientation of C_2H_5Br on GaAs(110). Temperature-programmed desorption measurements indicate that this species is molecularly adsorbed with a binding energy of 0.43 eV. After photoinduced C−Br bond cleavage two channels for ethyl fragments ejected are observed in the TOF: one resulting from direct ejection along the C−Br bond with a kinetic energy that varies from 0.6 to 1.1 eV, depending upon incident excitation wavelength, and the other, resulting from transient scattering from the surface potential energy well with a kinetic energy of 0.4 eV. Additionally, the kinetic energy of the directly ejected fragments varies with detection angle, a behavior consistent with a fragment−surface potential with normal energy scaling. The TOF measurements also indicate that, at coverages of <1 ML, the C_2H_5Br is oriented with the C−Br bond at an angle near 30° from the surface normal in the $[0\bar{1}]$ direction. This result is in accord with earlier NEXAFS and TOF measurements and ab initio calculations of CH_3Br on the same surface, which show that such a polar molecule is individually oriented by electrostatic interaction with the surface GaAs dipoles.

1. Introduction

Studies of the photofragmentation dynamics of weakly adsorbed molecules on single-crystal surfaces have provided useful insights into the process of adsorbate bond cleavage at surfaces.[1−3] For example, time-of-flight studies have shown that molecular bond cleavage following surface irradiation may occur as a result of photon absorption by the substrate and subsequent attachment of a "hot" electron to an adsorbate or through direct photon absorption by the adsorbate molecules.[4−11] The relative magnitude of these processes may vary with coverage and the precise energy of the exciting photon. These dissociative channels yield distinct photofragment kinetic energies, which, in the absence of collisional mixing, may be clearly observed using time-of-flight measurements.

One of the most striking dynamical effects has been that in many cases highly anisotropic angular distributions of fragments have been detected. These distributions have been shown clearly to reflect the local bonding orientation of the adsorbate molecule, allowing the possibility of employing angular resolved measurements as a probe of molecular surface alignment. From this perspective, the process may be regarded as a neutral-particle version of the desorption phenomena seen in ESDIAD.[12]

In this connection, several groups[8,9,11,13−15] have clearly shown that the ejection of light species, i.e., H or CH_3, can be used to probe molecular orientation on metal, semiconductor, and insulator substrates. For example, photoinitiated dissociation of CH_3X (X = Cl, Br, I) has been used to probe molecular orientation on two different corrugated semiconductor surfaces,[5,8,16,17] i.e., GaAs(110) and CdTe(110).

The present study attempts to investigate the applicability of the aforementioned technique to more complex adsorbate systems. For example, it is important to understand how the ejected fragment dynamics vary with increasing the carbon-chain length. The current study investigates the photointiated reactions of C_2H_5Br on GaAs(110), the next largest member of the brominated alkane family after methyl bromide. Furthermore, the gas-phase physics of C_2H_5Br are well documented as a result of numerous spectroscopic, electron attachment, and photofragmentation studies.[18−22] Knowledge of the behavior of the isolated molecule has proven to be very useful as a good starting point for understanding the photoreactions of the same weakly bound adsorbates.[4,5,8,11]

The (110) plane of GaAs is an attractive surface to use experimentally because its clean, reconstructed surface is readily prepared and its structure well characterized. Its asymmetrically corrugated surface allows examination of the role of atomic-scale microfacets on adsorbate orientation; in this connection it is the same substrate as that employed in the CH_3X studies mentioned above. For CH_3X molecules, adsorbate orientation has been found to originate primarily from electrostatic interactions between the permanent dipole of the adsorbate and a local surface dipole.[23] In addition, the use of GaAs allows comparison of our data with earlier photochemical and thermal chemical studies[24] of C_2H_5Cl on GaAs(100).

2. Experimental Section

Angle-resolved time-of-flight spectroscopy (TOF) and temperature-programmed desorption (TPD) were the primary tools used here to investigate the photodynamics of ethyl bromide on GaAs(110). The details of the experimental setup have been described elsewhere, and only a brief discussion will be provided.[5,25] All experiments were performed in an ultra-high vacuum (UHV) system with a main chamber that had a typical base pressure of 2×10^{-10} Torr. This chamber was also equipped with a quadrupole mass spectrometer (QMS) used for both TOF and TPD measurements, a LEED apparatus for measurement of crystal order and orientation, and an ion gun used for sputter cleaning the sample surface.

A single-crystal sample of GaAs(110) measuring $1 \times 1 \times 0.1$ cm with n-type ($2 \times 10^{17}/cm^3$) Si doping was mounted on a 0.125 mm thick strip of Mo foil. This sample was heated resistively and its temperature measured by a thermocouple spot-welded to the Mo foil near the middle of the sample. The sample assembly is also mounted in good thermal contact with and at the bottom of a liquid nitrogen reservoir. A clean surface was prepared by repeated cycles of sputtering with 500 eV Ar^+ ions at 300 K and subsequent annealing to 840 K. After surface

[⊗] Abstract published in *Advance ACS Abstracts,* October 1, 1997.

S1089-5647(97)01970-6 CCC: $14.00

preparation, a sharp (1 × 1) LEED pattern was observed. The quality of the sample surface was further ascertained by measuring a series of CH_3Br desorption spectra. Previous experiments have established the shape of these TPD curves in the absence of surface defects.[25] The determination of the [01] and [0$\bar{1}$] directions was accomplished through the use of the dynamic LEED procedure described in ref 26. All polar detection angles (θ) are measured from the surface normal and are defined as positive in the direction of the [01] surface vector.

The prepared sample was cooled to 90 K and then exposed to ethyl bromide using a pinhole doser consisting of a 0.1 mm circular opening at the end of a 6 mm diameter supply line. Before sample exposure, the 99+% pure ethyl bromide (Aldrich) was purified by several freeze−pump−thaw cycles so as to remove any volatile decomposition products.

TOF measurements were made by exposing the adsorbate-covered sample to 20 ns pulses of an unpolarized laser beam from an excimer laser operating at either 193, 248, or 351 nm. This beam was introduced through either of two fused silica windows on the main chamber such that its angle of incidence on the surface was at 60° with respect to the line of sight of the QMS. TOF spectra for different detection angles were recorded by rotating the sample manipulator relative to the QMS about an axis parallel to the $\langle 1\bar{1}0 \rangle$ direction. Spectra were taken every 5°; however, for graphical clarity not all of these data are presented in the figures below. All TOF spectra were normalized to take into account the absorbed photon density and the variation in the area illuminated and subtended by the detector as the sample is rotated.

To extract the dynamical quantities of the photofragment distributions (e.g., average kinetic energy), the TOF data were fit using a modified Maxwell−Boltzmann distribution. Numerous TOF studies have successfully employed this distribution to accurately fit their results.[27] A detailed account of this fitting procedure is given in refs 28 and 29. This procedure also transforms the raw TOF data, which is measured by the QMS as density, into flux. Thus, the area under the suitably transformed TOF peaks is proportional to the number of photofragments ejected into the solid angle subtended by the detector.

The fluence of the incident radiation was 0.2−0.7 mJ/cm^2. These low fluence levels were chosen for two reasons. First, low per-pulse desorption reduces photofragment collisions above the substrate−adsorbate interface due to the low desorbate density. The presence of such collisions would introduce velocity broadening in the TOF spectra as well as randomize the nascent angular distribution of the photofragments. In this connection, TOF signals scaled linearly with fluence, within experimental uncertainty, over the range 0.07−0.7 mJ/cm^2. The profile of the TOF signals was also unaltered for this fluence range. Typically, fluence values of ∼0.2−0.7 mJ/cm^2 were chosen because they afforded good signal-to-noise per pulse: values less than 0.2 mJ/cm^2 showed poor signal-to-noise characteristics. Second, numerical solutions to the heat equation showed that at these low levels the laser irradiation produced less than a 3 K temperature rise in the substrate,[30] thus eliminating the contribution of any laser-induced thermal desorption to the TOF signals. Finally, note that exposure of the adsorbate-covered surface to ∼1000 pulses at these low fluences (at 193 nm) resulted in only a small depletion (typically less than 10%) in the adlayer surface density, thereby minimizing the importance of concomitant chemical changes in the system during irradiation.

3. Results

This section presents the temperature-programmed desorption and time-of-flight measurements for the C_2H_5Br/GaAs(110) adlayer. The thermal desorption measurements show that this surface system exhibits characteristically different chemical behavior depending on whether or not it is exposed to UV light. The subsequent description of the TOF measurements provides insight into the fragment dynamics following irradiation.

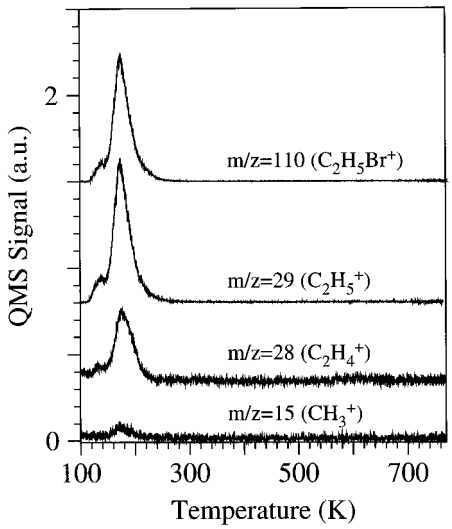

Figure 1. TPD spectra of different hydrocarbon species for an initial coverage of slightly less than 1.2 ML of C_2H_5Br on GaAs(110) show identical thermal desorption profiles with a peak desorption temperature of ∼175 K, indicating that this system exhibits simple molecular adsorption/desorption phenomena.

3.1. Adsorption and Photodissociation of Ethyl Bromide on GaAs(110). Before surface irradiation, the thermal chemistry of ethyl bromide on GaAs(110) was studied using temperature-programmed desorption (TPD). These studies were necessary to establish the nature of the adsorbed layer, i.e., island formation or layer-by-layer growth, and the chemical state of the adsorbed molecule. Desorption spectra were taken with a 5 K/s ramping speed over the temperature range 90−840 K. The data obtained clearly indicated that, in the absence of irradiation, ethyl bromide undergoes simple, nondissociative, adsorption/desorption on the GaAs(110) surface.

Representative TPD spectra are shown in Figure 1 for a surface dosed with a coverage of slightly less than 1.2 ML. The spectra have *m*/*z* values corresponding to the ions of the species C_2H_5Br, C_2H_5, CH_3, and C_2H_4. Each spectrum exhibits identical desorption profiles, indicating that all of these species originated from cracking of the parent molecule in the ionizer region of the QMS.

Figure 2 illustrates representative TPD spectra obtained at an *m*/*z* value corresponding to the parent molecule. Low exposures to ethyl bromide produce relatively narrow desorption profiles that peak at ∼200 K. With increasing coverage this peak not only grows in area, but its maximum shifts toward lower temperatures. Such a shift is characteristic of first-order desorption kinetics with significant adsorbate−adsorbate repulsive interactions. Similar behavior has been seen for CH_3X[25,31−37] adsorbed on bulk metals and insulators as well as on GaAs-(110). The shift can be accurately modeled by considering dipole−dipole interactions between oriented molecules.[25,38,39] With increasing coverage this feature saturates in intensity and remains at a peak temperature of 175 K. The saturation of this peak marks the completion of the first monolayer. Higher dosage yields a weak shoulder at 130 K, which can be seen more clearly in Figure 1. This shoulder can be interpreted as the formation of either a second layer or, possibly, a more compressed phase of the first layer. Reproducible single-monolayer coverage was obtained by exposing the sample to

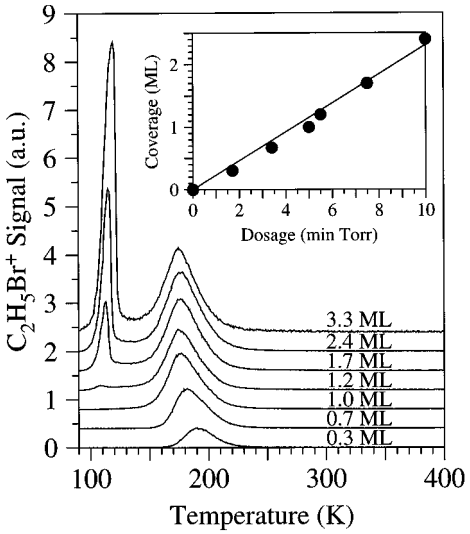

Figure 2. TPD spectra ($m/z = 110$) of C_2H_5Br desorbing from GaAs(110) at various initial coverages ranging from submonolayers to multilayers. The sticking coefficient is equal to 1 up to ~2.4 ML as suggested by the linear relation between the integrated TPD peak areas and dosing times (see inset).

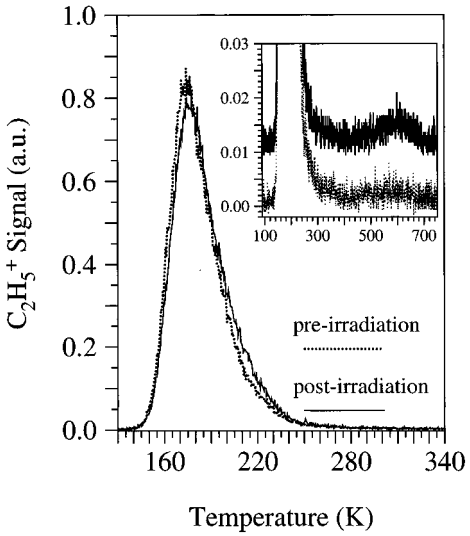

Figure 3. Comparison of the thermal desorption profile for 1 ML of C_2H_5Br ($m/z = 29$) before exposure to UV light and after irradiation with 536 pulses of 0.7 mJ/cm^2 at 193 nm light. There is a small yet noticeable depletion in the adlayer in addition to growth of a high-temperature feature after irradiation (see inset). The scale in the inset has been changed to more clearly show that the detection of ethyl species desorbing at ~616 K occurs only after irradiation. Curves in the inset are vertically offset for clarity.

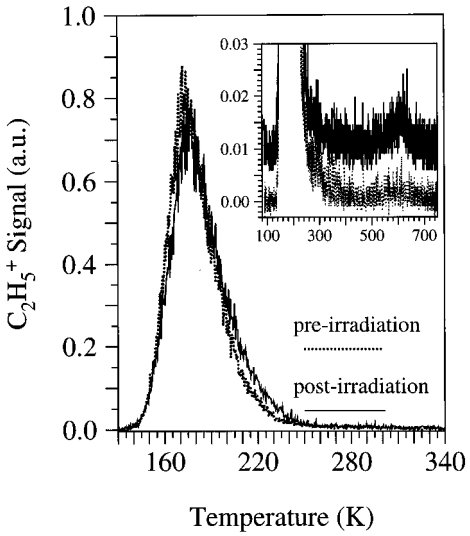

Figure 4. TPD of 1 ML of C_2H_5Br ($m/z = 29$) before and after illumination with ~5000 pulses of 0.35 mJ/cm^2 at 248 nm. Both the depletion in the adlayer and the appearance of a high-temperature peak at ~616 K (inset) were also observed after 193 nm radiation in the postirradiation TPD.

~1.5 ML and then annealing up to 140 K. The inset (Figure 2) shows that the area under the TPD curves is linear with dosage, indicating a constant sticking coefficient over the range shown.

Increasing the ethyl bromide coverage above 1 ML gives rise to a third feature in the TPD spectra at a significantly lower temperature, ~110 K. This peak does not saturate with increasing coverage; furthermore, close examination of all spectra containing this feature show that the spectra exhibit a common leading edge. Both of these observations suggest zero-order desorption kinetics corresponding to the sublimation of solid ethyl bromide, most likely in the form of islands.

Finally, small traces of GaBr were detected desorbing at temperatures greater than 500 K. A similar broad, small GaBr-derived feature had been observed following TPD from CH_3Br/GaAs(110). These earlier studies[25,29] attributed GaBr to reactions at defect sites, since the GaBr signal scaled approximately with the number of surface defects. The integrated area of the GaBr TPD feature in this work is very small compared to the intensity of the lower temperature features, again suggesting that this feature arises from minority defect sites. No other Ga- or Br-containing species were observed.

UV irradiation of the molecular overlayer induced significant chemical change in the adsorbed ethyl bromide. For example, Figure 3 shows two TPD spectra, at $m/z = 29$, of 1 ML layer, namely, the spectrum obtained before and after irradiation by 536 pulses of 0.7 mJ/cm^2 at 193 nm. It is apparent (Figure 3) that the UV exposure has caused a small reduction in the molecular desorption peak and that the peak desorption temperature has increased by ~2 K for the irradiated overlayer. This slight shift to higher desorption temperatures is consistent with a decrease in the dipole−dipole interactions of the adsorbates at lower coverages. The UV radiation has also introduced a weak but reproducible feature (inset of Figure 3) in the thermal desorption spectrum; this feature appears at much higher temperatures than the characteristic desorption temperature of ethyl bromide.

The above irradiation-induced changes occurred for each of the UV wavelengths used here. Figure 4 shows a TPD spectrum after a 1 ML layer was irradiated with 5000 pulses of 0.35 mJ/cm^2 at 248 nm. Note that virtually identical chemical changes are seen after exposure to either 193 or 248 nm radiation; compare Figures 3 and 4. However, a comparison of the integrated pre- and postirradiation data in Figures 3 and 4 also show that, to deplete roughly the same amount of the initial overlayer, approximately 6 times more photons are needed at 248 nm than at 193 nm. Similar chemical changes occurred when the overlayer was exposed to 351 nm radiation. However postirradiation TPD results following 351 nm illumination could not be precisely quantified due to the poor quality signals for radiation-induced desorbate products, which suggests a much lower cross section at this wavelength.

Closer inspection of the high-temperature desorption peaks from the irradiated overlayer enabled the UV-induced photochemical surface reactions to be identified. Figure 5 shows the TPD spectra of the surface-bound products that were observed after exposure to UV radiation. These spectra were obtained after one-fourth of the initial 1 ML was depleted using a fluence

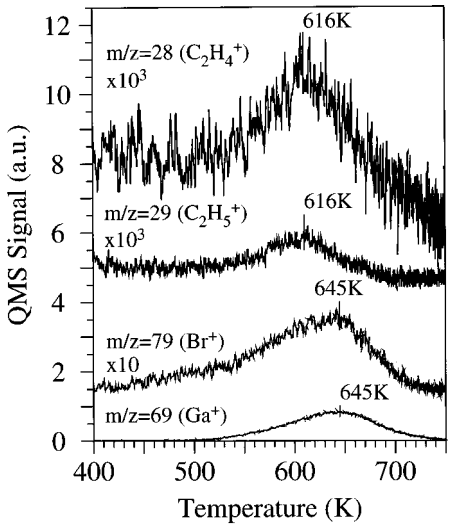

Figure 5. Thermal desorption products after 1 ML of C_2H_5Br was irradiated with 0.28 mJ/cm^2 at 193 nm. From the TPD spectra the desorption products are $GaBr_x$, desorbing at 645 K, and $C_2H_4^+$ and $C_2H_5^+$, desorbing at 616 K with identical thermal profiles.

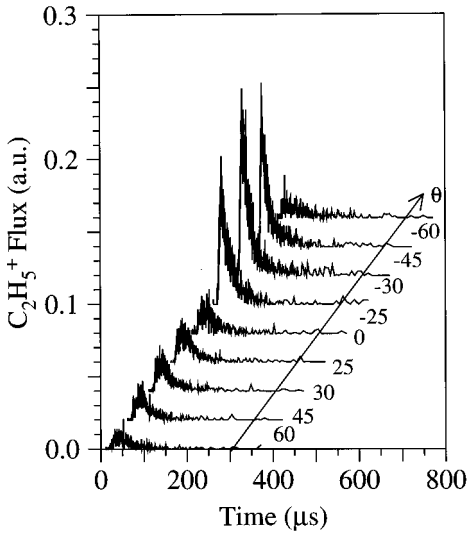

Figure 6. TOF spectra, taken at various detection angles with respect to the surface normal after 1 ML of C_2H_5Br was irradiated with 193 nm light, show a broad angular distribution. However a significant portion of the desorbate flux is detected in a much narrower (−20° to −50°) angular sector.

of 0.28 mJ/cm^2 at 193 nm. In obtaining much of the photoproduct TPD data, a relatively large fraction of the initial monolayer was dissociated in order to increase the signals from the radiation-induced desorbate species.

The photofragmentation of ethyl bromide molecules produced surface-bound hydrocarbon fragments as shown by the presence of a broad thermal desorption feature (500−700 K) for m/z = 29 and 28 peaked at ∼616 K. These m/z values correspond to ethyl radicals and ethene desorbates. After adjusting for the ∼5% contribution of cracked ethyl radical to the m/z = 28 peak,[24] the hydrocarbon distribution is estimated to be 14% ethyl radicals and 86% ethene. No higher mass hydrocarbons, e.g., m/z = 30 (ethane) and m/z = 58 (butane), were observed to desorb, even after heating to 840 K.

The high desorption temperature, ∼600 K, indicates that these fragments are rather strongly bound to the surface. The ethene desorption peak was analyzed using the peak width method proposed by Chan et al.[40,41] to estimate the desorption activation energy, E_d. Assuming first-order kinetics and coverage-independent values for the peak desorption temperature (616 K) and peak half-width (106 K) taken from the ethene desorption spectrum in Figure 5, a value of E_d = 67 kJ/mol is estimated. The amount of desorbed ethene on heating scaled roughly with the incident photon exposure.

In addition, a broad 500−750 K feature appeared, peaked at 645 K for both m/z = 69 and m/z = 79 corresponding to Ga and Br ions, respectively. Each of these signals exhibits identical postirradiation thermal desorption profiles, indicating photoinduced production of GaBr, $GaBr_2$, and/or $GaBr_3$. The absolute magnitude of these signals was significantly larger (5 times) than those associated with $GaBr_x$ formed on defect sites in the absence of irradiation.

3.2. Angle-Resolved Time-of-Flight Measurements. After characterizing the low-coverage adsorption and photochemistry of the ethyl bromide layer, angle-resolved time-of-flight spectroscopy was employed to study the photodynamics and molecular orientation of the adsorbate system. Adlayers of 1 ML thickness were irradiated with UV light of 193, 248, and 351 nm wavelength. At each wavelength TOF spectra were taken over a range of angles (θ) with respect to the surface normal. As stated earlier, the total amount of photodissociation was monitored with postirradiation TPD so as to ensure that <10% of the monolayer was depleted, thus causing the surface not to be substantially altered during the exposure.

Ethyl radicals were the only directly ejected fragments observed upon irradiation of the adlayer. Estimates made by measurement of postirradiation TPD peak areas showed that ∼60% of the photodissociated adsorbates are directly ejected ethyl radicals. In addition, a small fraction (relative to the observed ethyl fragments) of intact ethyl bromide molecules were also detected at very low kinetic energies. These molecular desorbates most probably originate from a desorption channel in which an energetic fragment undergoes a direct collision with an adsorbate. A simple calculation, based on hard-sphere collisions having kinetic energies that are typical of the photofragments, suggests that the kinetic energies of the fragments would be sufficient to desorb physisorbed ethyl bromide. However, such collisions would need to have small impact parameters to be effective, making them a relatively improbable event given the molecular orientation (discussed below) on the surface. Since fragment dynamics and chemistry are the main focus of this paper, this process will not be discussed further here.

Figure 6 shows the angle-resolved TOF spectra for 193 nm irradiation at various polar angles. A broad angular distribution of the ethyl photofragments is observed. In addition, the photofragmented ethyl radical distribution contains a narrow angular lobe directed between −20° and −50° with a maximum peaked sharply at ∼−30°. Very similar angle-resolved TOF distributions were observed for photodissociation at 248 and 351 nm.

Inspection of the TOF data suggests there is a strong correlation between fragment energy and angular distribution. For example, Figure 7 shows the TOF profiles, transformed into velocity space, for θ = −30° and 30° using 193 nm radiation. The TOF feature for θ = 30° is relatively symmetric about a velocity of 0.16 cm/μs (0.40 eV). This same peak profile is exhibited by all TOF spectra taken at positive detection angles.

However, for detection angles between −20° and −50° the TOF spectra are more intense and have higher peak kinetic energies than at the corresponding positive angles. For example, Figure 7 shows that the velocity distribution at θ = −30° is more intense at higher velocities than for the distribution at θ = 30°. But there are also similarities between the two TOF distributions. The figure shows that the low-velocity tails of

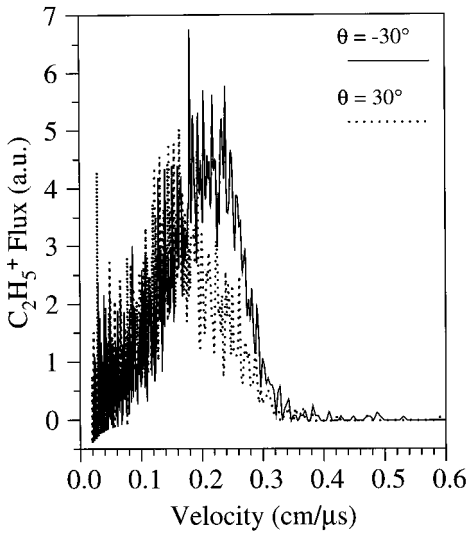

Figure 7. Comparison of TOF spectra at $\theta = -30°$ and $\theta = 30°$ for 1 ML of C_2H_5Br irradiated with 193 nm. The TOF spectrum for $\theta = 30°$ has been scaled to show the strong overlap in the rising edge at the two different detection angles. Also note that at higher velocities the ethyl flux is more intense for $\theta = -30°$.

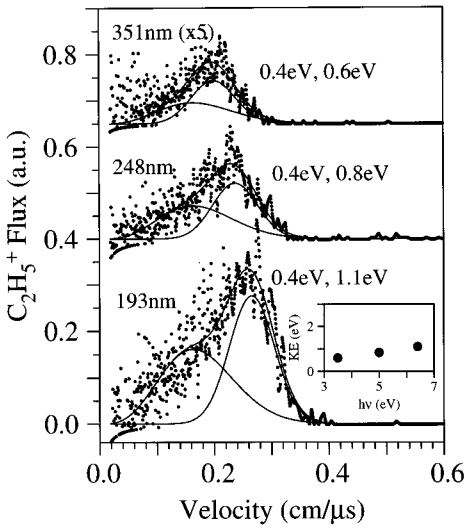

Figure 8. TOF spectra of 1 ML of C_2H_5Br taken at $\theta = -45°$ when illuminated with UV light at 193, 248, and 351 nm can be described by the sum of two modified Maxwell−Boltzmann distributions: one with a peak energy of 0.4 eV and the other with a peak energy that varies weakly with the incident photon energy ($h\nu$) (see inset).

the TOF features overlap for $\theta = 30°$ and $\theta = -30°$; this overlap of the low-velocity portion of the distribution was observed at all polar angles, positive and negative. These observations suggested that the TOF features for angles between $-20°$ and $-50°$ might be described by two or more distinct velocity distributions.

Careful examination of the time-of-flight and angular data shows that a good fit of the data at any angle might be made using a sum of modified Maxwell−Boltzmann distributions. Least-squares curve fitting reveals that an accurate global representation of the data can be obtained by using the following function consisting of the sum of two such distributions:

$$f(v,\theta) = A_s v^3 \exp\{-[(v-\beta_s)/\alpha_s]^2\} + A_f v^3 \exp\{-[(v-\beta_f)/\alpha_f]^2\}$$

where $f(v,\theta)$ is the ethyl fragment flux velocity distribution at angle θ. Here, α_i and β_i (i = f (fast) or s (slow)) are fitting parameters that determine the width and peak velocity for each Maxwell−Boltzmann distribution. The coefficients A_f and A_s depend only on the angle, θ, and determine the relative weight of each velocity distribution at a particular angle. Examples of the results of this fitting procedure are illustrated in data for $\theta = -45°$ shown by the solid lines in Figure 8. At this particular angle (in the $[0\bar{1}]$ direction), fragments are produced with two characteristic velocity distributions: a broader distribution peaked at low velocities and a narrower distribution peaked at higher velocities. The $\theta = -45°$ data are shown for the three wavelengths studied here; the peak of the slow distribution is independent of laser wavelength while the peak energy of the fast channel moves to somewhat higher energies as the photon energy is increased from 3.5 eV (351 nm) to 6.4 eV (193 nm). The inset of Figure 8 shows the dependence of the fast channel on photon energy. Note that only a relatively small fraction of the additional available energy appears in fragment translational energy as the photon energy is increased; the dynamical implications of this behavior are discussed below.

It was possible to use constant values of α_s, α_f, and β_s to fit data at all angles (for a given laser wavelength). However, it was found that the best fit required that β_f increase with increasing θ. This observation suggests that the peak velocity of the fragments produced in the "fast" channel is larger at angles further from the surface normal.

Also of interest are the values of A_f and A_s that are required to fit the data at a given angle. The required functional form of $A_f(\theta)$ is sharply peaked around $\theta = -30°$. At positive values of the polar angles (in the [01] direction) the fast distribution makes little or no contribution to the fragment flux. This point is evident in Figure 7 where the raw data for $\theta = 30°$ and $\theta = -30°$ are shown. By examining the angular dependence of the integrated velocity−flux distributions for the "slow" channel after the contribution of the "fast" channel has been subtracted from the TOF, it is found that the coefficient A_s varies as $\cos^2 \theta$ for both 193 and 248 nm laser irradiation. While this same behavior is apparent in the 351 nm data, the inadequate signal-to-noise level at this wavelength prohibited quantitative analysis. Similarly, by subtracting out the flux contribution from the "slow" channel, it was possible to extract a velocity-averaged angular flux distribution for the "fast" channel. The result of this analysis is given in Figure 9 for 193 and 248 nm laser wavelengths.

It seems appropriate, therefore, to regard the photofragmentation process as occurring via two dynamically distinct channels: one producing less energetic fragments with an angular distribution that is isotropic with respect to the surface normal and the other being more energetic and exhibiting strong angular peaking near $\theta = -30°$.

4. Discussion

The TPD data in Figure 1 show that, in the absence of irradiation, ethyl bromide undergoes only molecular adsorption and desorption on a defect-free GaAs(110) surface. However, both TPD and TOF measurements show that molecularly adsorbed ethyl bromide undergoes bond cleavage in the presence of ultraviolet irradiation.

It will be argued below that this photofragmentation of adsorbed ethyl bromide occurs via dissociative electron attachment (DEA) rather than through direct photon absorption by the adsorbate. Earlier work in this lab suggested that DEA is also the primary mechanism for photoinduced fragmentation of methyl halides on GaAs(110).[4,5,8,16] For ethyl bromide, three dynamically distinct channels appear to be the result of photoinduced DEA: two channels resulting in direct ejection

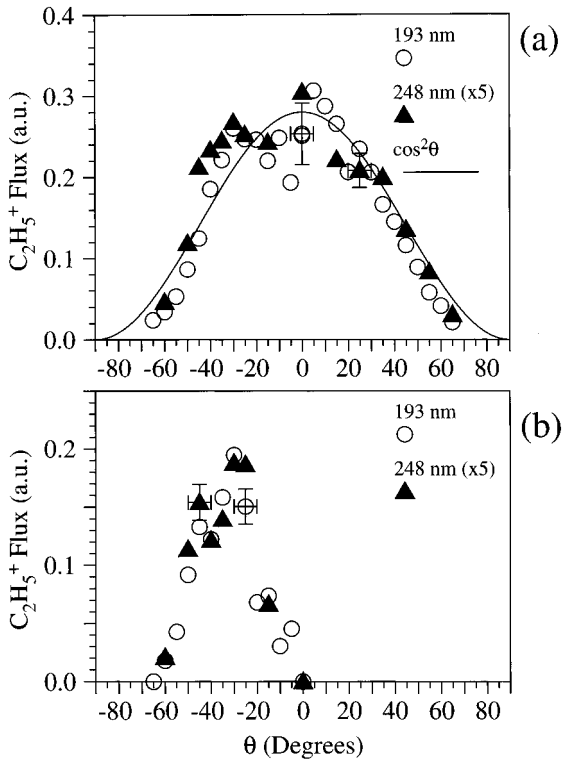

Figure 9. Total integrated ethyl flux as a function of detection angle for 193 and 248 nm light as derived from the fitting procedure described in the text for the "slow" channel, panel a, and the "fast" channel, panel b. The angular distribution for the "slow" channel, panel a, follows a $\cos^2\theta$ trend whereas the angular distribution for the "fast" channel is sharply peaked at $\theta = -30°$.

of ethyl fragments from the surface and one channel where the ethyl fragments become trapped on the surface. In no case is the ejection of Br into the vacuum observed, suggesting that this fragment becomes energetically accommodated at the surface, eventually forming a strong bond with the surface. Below we present arguments in support of the above mechanism and discuss some of the implications of the observed dissociation dynamics.

4.1. Dissociative Electron Attachment (DEA) vs Direct UV Photolysis. Before arguing in support of a DEA mechanism, it is important to assess the role of direct photon absorption by the adsorbate as the initiating step of the carbon−bromine bond rupture. UV photon absorption in alkyl halide molecules can occur via promotion of an electron from a nonbonding orbital primarily located on the halogen to an antibonding σ^* orbital. In ethyl bromide, UV absorption occurs in the range ∼300 nm (4.1 eV) to ∼185 nm (6.7 eV), resulting in C−Br bond rupture.

Many recent studies have shown that direct photolysis of molecules adsorbed on a metal or semiconductor surface is strongly quenched for low coverages ∼1 ML.[2,4,5,8,13,16,17,24] On these surfaces a strong coupling exists between the excited state and the substrate, allowing for efficient relaxation through electron−hole pair formation.[2,5,17] For example, it was shown in previous studies of CH_3Br on GaAs(110)[5,8] that direct photon-induced dissociation does not occur for coverages <1 ML.

Our observation of C−Br bond cleavage for 351 nm (3.5 eV) photons illustrates that direct photon absorption is unlikely to play a role in the photofragmentation. The ethyl bromide UV spectrum would need to be significantly (0.6 eV) red-shifted upon adsorption for 351 nm photons to be absorbed. An analysis of our TPD spectra using the Redhead equation[43] shows that the surface binding energy is a weak 41 kJ/mol (0.43 eV). Other studies have shown that the UV absorption spectrum remains essentially unchanged upon weak surface adsorption.[11] As the UV spectra of methyl and ethyl bromide are nearly identical, direct photon absorption can also be ruled out for the latter species.

Instead, prior studies of the photoreactions for molecules in the first monolayer on metal or semiconductor surfaces have attributed the reactions exclusively to substrate-mediated electron-induced bond cleavage. For example, in the case of CH_3Br on GaAs(110)[5,8] or Pt(111)[44] the reaction is known to occur via DEA. Evidence for substrate-mediated C−Cl bond cleavage at low coverages has also been observed for C_2H_5Cl on metal crystals[45,46] and GaAs(100).[24]

Ethyl bromide, like many other alkyl halides, has a strong propensity to undergo DEA in the gas phase. When adsorbed on GaAs(110), the energetics of ethyl bromide[2,5,8,13] DEA is thought to occur as follows: Absorption of UV photons (⩾3.5 eV) by the substrate results in the promotion of electrons across the 1.4 eV bandgap into the conduction band. Depending on their energies, these electrons either pass over or tunnel through any surface barrier and attach to an adsorbed ethyl bromide molecule to form a molecular negative-ion resonance which can dissociate into an ethyl radical and a Br^- ion. This process is directly analogous to that observed in the gas phase after attachment of electrons with energies less than 2 eV.

As described elsewhere,[2,5,8,13] the expected energetics for the DEA process is generally consistent with the range of photon energies used here. Since the photoemission threshold for GaAs(110) is ∼5.6 eV, photon energies in excess of 6.86 eV would be required to eject an electron for attachment to an isolated gas-phase molecule of C_2H_5Br having a vertical attachment energy[61] of 1.26 eV.[47] However, the affinity level of the molecule is perturbed upon adsorption, and the energetics must also include the reduction in this energy due to adsorbate−surface image-charge stabilization, ∼1 eV, and adsorbate−adsorbate interactions, ∼0.6 eV.[5,13,18] In addition, the work function of an alkyl halide-covered surface (with halide-down molecular orientation) is expected to be lowered by ∼1.5 eV, based on the observations of White and co-workers[2] on the CH_3Br/Pt(111) system. The combination of these effects lowers the estimated electron attachment energy by ∼3.1 eV, to give a minimum photon energy of ∼3.8 eV. The affinity level in the isolated molecule is observed to have a width of 1−2 eV in the gas phase;[47,48] this width is expected to be even larger in the adsorbed state due to adsorbate−surface interactions.[49] Thus, our observation of DEA for 3.5 eV photons seems reasonable due to the combination of the above effects.

4.2. Dynamics of Ethyl Photofragments. Given that substrate-mediated DEA is the most plausible mechanism for the formation of ethyl radicals and bromine ions, the fate of the ethyl fragments produced is now considered. The two channels that produce directly ejected ethyl radicals are distinguished by their TOF and angular distributions. A "fast" channel produces ethyl radicals with peak kinetic energies in the 0.6−1.1 eV range, depending on the photon energy. The angular distribution for this channel is independent of photon energy and sharply peaked at a polar angle near −30°. Previous studies[8,16] have interpreted the anisotropic angular distributions produced by similar systems to be indicative of the preexcitation orientation of the adsorbate molecule on the corrugated semiconductor surface. The angular distributions observed in the present experiment suggest that the R−Br bond axis of the unexcited ethyl bromide molecule is tilted at 30° with respect to the surface normal in the [0$\bar{1}$] direction.

There are several possible explanations for the occurrence of the "slow" (peak energy ∼ 0.4 eV), angularly symmetric

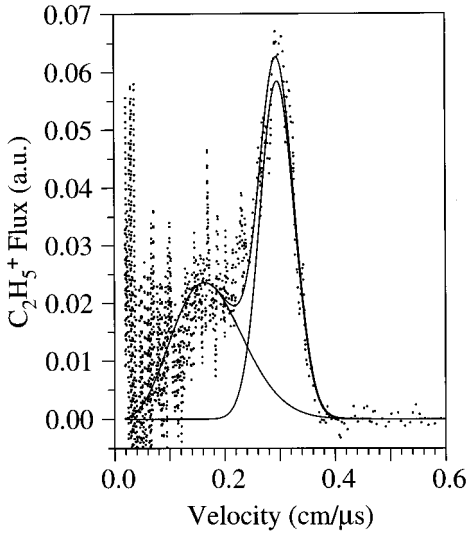

Figure 10. TOF spectrum for 0.17 ML taken at $\theta = -45°$ for 193 nm illumination. As discussed in the text, the contribution to the total ethyl photofragment flux from the "slow" channel is approximately the same at 0.17 and 1 ML.

feature in the TOF spectra. First, and perhaps the most obvious, is that this feature originates from ethyl photofragments that have undergone inelastic collisions with surrounding, adsorbed, ethyl bromide molecules on their exit trajectory. Such an interpretation would be consistent with the $\cos^2(\theta)$ distribution observed (see Figure 9a) for these ethyl radicals, implying that the initial directional character of the photofragmentation process has been subsequently randomized.

However, comparison of the TOF spectra at high, i.e., ~1 ML, and low coverage showed that the magnitude of the "slow" feature is not significantly diminished at lower coverages where one might expect, in the absence of overlayer island formation, interadsorbate collisional events to be minimized. For example, Figure 10 shows the TOF spectrum for 0.17 ML coverage, which was obtained by averaging seven individual spectra. A comparison of the integrated signal in the "fast" and "slow" peak indicated that at this coverage 44% of the total desorbed ethyl photofragments detected at −45° were associated with the "slow" TOF feature. This value is close to the 49% observed for 1 ML at the same detection angle. These results suggest that velocity randomization by fragment−adsorbate collisions is not the origin of the relatively large proportion of ethyl photofragments produced in the "slow" channel.

A second mechanism is possible due to the fast quenching processes on metals and semiconductors: adsorbate molecules might relax into a highly vibrationally excited ground electronic state after an initial negative-ion state has been quenched. The energy gained could result in vibrational predissociation of the surface-bound ethyl bromide. Such a process has been previously proposed as one of the channels for photoinduced dissociation of ethyl chloride on Ag(111).[46]

However, in our case, it seems unlikely that quenching of the ion state would create sufficient residual vibrational excitation to break the C−Br bond. From the gas-phase measurements mentioned above, it is known that the vertical attachment energy (VAE) of ethyl bromide is 1.26 eV with a width of 1−2 eV.[20,21,47] This value is much lower than the ~3 eV dissociation energy of neutral ethyl bromide. Therefore, it is very unlikely that on relaxation to the ground-state potential energy surface the adsorbed molecule, which has even a lower VAE, will have enough energy to surmount the ground-state dissociation well. Furthermore, the above mechanism can be dismissed as being responsible for the slow TOF feature on the basis that a similar feature was not observed in the CH_3Br/GaAs(110) system.

Finally, a channel for very significant energy accommodation between the photofragment and the substrate surface must be present as evidenced by the capture of a substantial fraction of the ethyl fragments on the surface following photodissociation. The existence of such an attractive well for ethyl fragments in the near-surface region could explain both the "slow" direct channel and the relatively large number of ethyl fragments trapped on the surface. This process would be analogous to the trapping/desorption phenomenon sometimes observed when atoms or molecules in a molecular beam scatter from a surface.[50]

The existence of such an attractive surface well for ethyl fragments in conjunction with electron-mediated bond cleavage is consistent with most of the observations made here. The origin of each of three dynamically distinct channels occurs when an ethyl bromide molecule, adsorbed on the surface with its bromine end "down" and with the C−Br bond tilted away from the surface normal in the $[0\bar{1}]$ direction, captures an electron in its σ^* orbital. This event causes an impulsive force to act along the C−Br bond; in the gas phase this process results in a broad distribution of fragment translational and internal energies. Those fragments formed with enough kinetic energy in the proper coordinates to surmount the near-surface barrier will be directly ejected into the vacuum, thus giving rise to the "fast" channel observed here. Other fragments may lack sufficient initial kinetic energy in this critical coordinate(s) but possess sufficient total energy to surmount the barrier. These fragments sample the near-surface well, until eventually escaping the well when energy is redistributed into the proper coordinate(s)—providing that the rate of energy loss to the surface is not very large during the time the fragments are in the near-surface region. One would expect these fragments to have less kinetic energy and an angular distribution that would not reflect the initial orientation; this is exactly what is observed for the "slow" channel. Finally, some fragments either do not have enough energy to ever escape the surface or lose sufficient energy in the time spent sampling the well that they become trapped at the surface.

While one might expect that the dynamics of a polyatomic molecule interacting with a rather corrugated semiconductor surface could only be described by a complex multidimensional potential energy surface, it is interesting to note that these results are also consistent with an attractive ethyl−surface potential that is roughly one-dimensional. Specifically, if the attractive well for the ethyl−surface potential is only dependent on the normal component of the translational energy, then two further observations can be explained. First, the flux of fragments from the "slow" channel has a roughly $\cos^2(\theta)$ (Figure 9a) angular distribution, which is consistent with normal-energy scaling (providing the fragments have attained a somewhat statistical energy distribution while in the near surface region).[51,52] Angular distributions of the type $\cos^n(\theta)$ with $n > 1$ have been observed for angle-resolved TPD studies where a similar one-dimensional potential is expected.[51] Also, a shift to higher peak translational energy in the fragments from the "fast" channel is observed as the detection angle is shifted away from the surface normal (Figure 11). Consider a case where the impulsive force due to DEA acts along the C−Br bond and where these bonds have some instantaneous orientation with respect to the surface normal. If only the component of momentum in the direction normal to the surface is effective at surmounting the barrier, then the adsorbates, with C−Br bond tilted at directions further from the surface normal, will require a larger amount of total energy to escape from the surface. Because we measure the

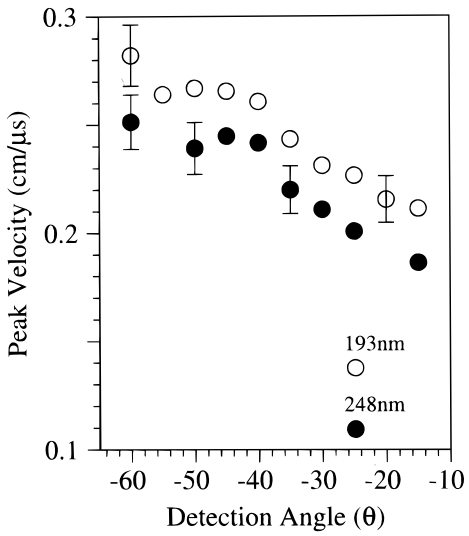

Figure 11. Peak velocity of the "fast" channel decreases for detection angles closer to the surface normal. This trend is observed at both 193 and 248 nm illumination.

speed distribution in the lab frame (at a given polar angle), the most probable speed in the fragment velocity distributions could increase as the detection angle is increased as a consequence of normal energy scaling.

Recently, Polanyi and co-workers[60] have observed similar fast and slow channels for the photodissociation of methyl bromide on alkali halide surfaces. The dynamics in their work originates from photon absorption by the adsorbate followed by direct ejection or energetic collisions of methyl fragments with adjacent adsorbates. They have established a strong coverage dependence for the orientation of the C−Br bond, with the bond axis parallel to the surface at low coverage. The lack of strong coverage dependence (Figure 10) in our velocity and angular distributions argues for a different origin for the dynamics of the C_2H_5Br/GaAs(110) system.

In the previous TOF/UV photodissociation studies of CH_3Br/GaAs(110) carried out in our laboratory, only fast, angularly peaked methyl fragment distributions were observed. The mechanism for the production of the methyl photofragments was attributed to a direct impulsive process involving DEA; no evidence for a "slow" or trapping channel was observed. An attractive well for methyl−surface interactions may also exist, but the average translational energies imparted to the methyl fragments may be large enough to prevent observation of "slow" and trapping channels.

Comparative studies of fragment energy partitioning made in gas-phase photodissociation of alkyl halides support these general arguments.[42,53−55] Specifically, it is seen that a smaller fraction of the total available energy is transferred to the translational energy of the fragments as the size of the alkyl group is increased. For example, one study[53] showed that the fraction of available energy deposited internally for methyl, ethyl, and propyl iodides was 17%, 39%, and 54%, respectively, when the ground state of iodine was formed via 248 nm photodissociation. A similar trend should hold for the DEA fragmentation in the same series of alkyl halides; in photodissociation an electron is transferred from an essentially nonbonding orbital to the antibonding σ^* orbital while in DEA the electron is supplied to the same σ^* orbital from an external source. This parallel was drawn many years ago in the interpretation of crossed-molecular-beam studies where a halogen is transferred from an alkyl halide to an alkali metal atom via the harpooning mechanism.[56]

Returning to our measured angularly resolved TOF spectra for C_2H_5Br, we observe a small shift in peak translational energy with increasing polar angle; this is attributed above to an attractive potential with normal-energy scaling (Figure 11). Note that if such a potential exists, the peak of the observed angular distribution may not accurately reflect the original adsorbate orientation on the surface. A given angular distribution of nascent photofragment flux would have its peak shifted to smaller polar angles due to the refractive effect of the potential. NEXAFS studies on the CH_3Br/GaAs(110) system have determined that the C−Br bond in the molecular adsorbate is oriented at $-45 \pm 5°$ with respect to the surface normal.[16] In the same study, the angular distribution for methyl photofragments was also found to be peaked near −45°; in this case it appears that any surface potential that may exist produces a negligible shift in the photofragment angular distribution. In the present work, an angular distribution for ethyl fragments peaked near −30° is found. This shift in the angular distribution toward the surface normal (when compared with the CH_3Br case) could be due to the refractive effect of the surface potential and/or a different initial orientation of ethyl bromide on the surface. Without additional confirming measurements using a probe that is sensitive to the initial molecular orientation on the surface, the role of the surface potential in this shift cannot be assessed.

Harrison and co-workers have studied methyl bromide UV photofragmentation on Pt(111) and have also observed an increase in the peak translational energy as the polar angle of detection is increased.[13] They propose that the origin of this shift is a repulsive interaction of the electron in the antibonding orbital (primarily localized on the methyl group) when the C−Br bond axis is closer to the substrate electron density. While this may seem plausible in the absence of other evidence, we propose here that an interaction with roughly normal-energy scaling is more consistent with the totality of the observations presented here.

4.3. Chemistry of the Trapped Ethyl Fragments. This section discusses the thermal chemistry of the ethyl fragments trapped on the surface following photofragmentation. Prior studies by White and co-workers on the photoreactions of molecularly adsorbed methyl and ethyl halides on metal surfaces, i.e., Pt(111)[44,45] and Ag(111),[46,57,58] had shown that photoinduced C−Cl bond cleavage produced surface-bound methyl and ethyl species and halide atoms. In contrast, for the case of alkyl halides on GaAs surfaces, no evidence has been seen for the retention of methyl groups on the surface following surface irradiation of adsorbed CH_3X,[5,8] but one prior study reports significant capture of C_2H_5 groups.[24] This observation is also in accord with the stronger role of the proposed surface potential in the case of C_2H_5 dynamics described above for our (110) sample. Specifically, Liberman et al.[24] reported that on exposure to UV radiation ethyl chloride, which is molecularly adsorbed on Ga-rich GaAs(100), dissociates to produce surface-bound ethyl radicals and Cl atoms: an observation that closely parallels our results of ethyl bromide on the (110) surface of GaAs. Since these two GaAs surfaces have very different stoichiometry, a comparison of the reactions on the two surfaces can give useful information on the thermal reaction site.

In the work described in ref 24, the ethyl fragments bound to the Ga-rich (100) surface of GaAs underwent β-hydride elimination to yield ethene. Similarly, in our experiments, TPD signals are observed for ethene and ethyl radicals desorbed from an irradiated C_2H_5Br layer on GaAs(110). The ethene peak desorption temperature of 616 K that was observed on the (110) surface agrees well with the 614 K peak desorption temperature assigned to the formation of ethene via β-hydride elimination

on the (100) Ga-rich surface of ref 24. The close agreement in desorption temperatures from the two surfaces indirectly suggests that the ethene desorbing from the GaAs(110) surface is also a consequence of surface-bound ethyl fragments undergoing β-hydride elimination.

Prior studies of desorption from the ethyl-terminated surface of Ga-rich and As-rich GaAs(100)[59] are relevant to these observations since ethene is produced on both surfaces via β-hydride elimination. In this case, the ethyl termination was provided by thermal reaction of the surface with $(C_2H_5)_3Ga$. This study found that β-hydride elimination was inhibited on an As-rich surface when compared with a Ga-rich surface. Specifically, a greater percentage yield of ethyl fragments were detected desorbing from the As-terminated GaAs(100) surface than ethene or hydrogen. Consequently, the presence of As atoms on the (110) surface appears to make ethyl radical desorption more competitive with the β-hydride elimination reaction. In addition, the fact that the ~620 K peak desorption temperature for ethene from the Ga-rich surface is in much better agreement with our result than the 30 K lower desorption temperature on the As-rich surface also suggests that the ethyl fragments are preferentially bound to Ga surface atoms.

Finally, in the study conducted by Liberman et al.[24] on ethyl chloride-covered Ga-rich GaAs(100), ethane desorption was observed at 614 K following irradiation. This channel was ascribed to the reaction of adsorbed atomic hydrogen, perhaps originating from the β-hydride elimination channel, with surface-bound ethyl fragments to produce ethane. However, evidence of this reaction was not seen on the GaAs(110) surface. In the study on Ga-rich GaAs(100), it was estimated that only 20% of the total hydrocarbons desorbed from the surface were in the form of ethane whereas 70% were ethene molecules and only 10% ethyl radicals. Thus, it is plausible that an increase in ethyl radical desorption would come about at the expense of the ethane reaction channel. Perhaps an abundance of As sites suppresses the mobility of surface hydrogen and thereby suppresses the rate of ethane production on all but Ga-rich surfaces.

5. Conclusion

TPD and angle-resolved TOF measurements have revealed that ethyl bromide adsorbed on GaAs(110) appears to have three dynamically distinct channels for UV-initiated carbon−halogen bond rupture. While one might expect the photodynamics of this system to be similar to that of the previously studied and closely related CH_3Br/GaAs(110) system, the results presented show that there are considerable differences between these two alkyl halide systems. Specifically, only the "fast" channel for ethyl bromide photodissociation shares the highly peaked anisotropic angular distributions observed in the methyl bromide studies: these anisotropic angular distributions are taken to reflect the molecular orientation on the surface prior to photofragmentation.

Ab initio cluster calculations have been performed by Black et al.[23] to model the methyl bromide/GaAs(110) system. These calculations show that a significant fraction of the adsorbate/surface attraction arises from the interaction of the molecular dipole moment with dipole resulting from charge separation between the Ga and As species in the surface.[23] The resulting stable configuration has the C−Br bond axis tilted at ~−50° from the surface normal with the halogen end down. This calculated orientation is in good agreement with angle-resolved TOF studies for CH_3Br/GaAs(110).[5,8] Given that ethyl bromide has a molecular dipole moment of similar magnitude to that of methyl bromide, we could expect a similar orientation for ethyl bromide. This molecular surface orientation is consistent with the dynamical observations for the "fast" channel discussed above.

The "slow" and postirradiation trapping channels observed here for ethyl fragments do not have counterparts in the previous methyl bromide work. Instead, the observation of these two channels is attributed to the presence of a potential barrier that the ethyl fragment must surmount to escape from the surface. Such a barrier could also exist for methyl fragments in the near-surface region. However, it is proposed that, in the case of CH_3Br, virtually all fragments have sufficient kinetic energy to escape from the surface directly. But ethyl fragments are produced with a smaller fraction of the total available energy partitioned into translation, thereby enhancing the ability of the potential well to capture or scramble the velocity of the ethyl fragments. Gas-phase studies of alkyl halide photodissociation suggest that the fraction of total energy available to the fragments in the form of translation decreases from ~90% to ~60% when the methyl group is switched to ethyl, supporting our observations. The average translational energy available to larger alkyl fragments should even be less; propyl (and larger) fragments might show a further enhancement of the effect of this proposed trapping potential.

Observation of both "fast" and "slow" channels for the ethyl photofragments, each with a distinct angular distribution, brings to mind the results for molecular beam/surface scattering studies with direct scattering and trapping-desorption channels. While it may be satisfying to imagine the nascent ethyl photofragment to be somewhat analogous to a "half-reaction" being initiated by the DEA process, it is clear that the analogy should not be taken too far. Even though the ethyl radicals may have a narrow range of initial angular orientations (perhaps determined by the libration of the parent molecule about some low-energy configuration), they appear to be produced with a wide range of internal and translational kinetic energies. In addition, fragments on various trajectories may experience a range of different potential barrier heights, depending on the fragment orientation with respect to a highly anisotropic surface. This suggests that the dynamics observed will be highly averaged quantities. That energy and angular distributions are observed that are consistent with a simple one-dimensional normal-energy scaling perhaps reflects this averaging. It should also be noted that the ethyl fragments, when given their initial impulse in the DEA process, are located at some distance from the GaAs surface (about 0.5 nm); the simple one-dimensional nature of the observed interaction may be due to the fact that the fragments only experience the long-range part of the interaction potential which should have smoother isocontours as the fragment−surface distance becomes large. By extending these studies to propyl bromide and larger alkyl bromides, we hope to further assess the dynamical implications of this model.

Because ethyl fragments become trapped on the surface, this work also provides a method for the study of the bonding and chemistry of species that cannot be dosed onto a surface in the usual way. It is interesting to note that the ethyl photofragments produced on Pt(111)[45] result in ethene, ethane, and hydrogen production on heating−identical with what was observed on Ga-rich GaAs(100). However, consistent with its weaker dehydrogenation catalytic properties, the ethyl fragments on Ag(111)[46] recombine on heating to produce butane. These observations suggest that GaAs(110) falls in the middle of this spectrum of catalytic behavior for dehydrogenation of surface-bound ethyl radicals. Comparisons of this behavior with other surfaces of GaAs that are either As- or Ga-rich suggest that dehydrogenation is controlled by the Ga/As ratio. Future work

with other alkyl halides (possibly on other semiconductor substrates) may also help us to elucidate the thermal chemistry of alkyl radicals on semiconductor surfaces.

Acknowledgment. We thank Prof. George Flynn for useful comments on this work. In addition, we are greatly appreciative of the careful review and extensive comments by Dr. Nicholas Camillone. We also acknowledge support of this work by DOE under Contract DEFG0290ER14104 and partial instrumentation support by JSEP under Contract DAAL0391C0016.

References and Notes

(1) Avouris, Ph. *Acc. Chem. Res.* **1995**, *28*, 95.
(2) Zhou, X. L.; Zhu, X. Y.; White, J. M. *Surf. Sci. Rep.* **1991**, *13*, 76.
(3) Chuang, T. J. *Surf. Sci. Rep.* **1983**, *1*, 1.
(4) Yang, Q. Y.; Schwarz, W. N.; Osgood, Jr., R. M. *J. Chem. Phys.* **1993**, *98*, 10085.
(5) Yang, Q. Y.; Schwarz, W. N.; Lasky, P. J.; Hood, S. C.; Loo, N. L.; Osgood, Jr., R. M. *Phys. Rev. Lett.* **1994**, *72*, 3068.
(6) Marsh, E. P.; Tabares, F. L.; Schneider, M. R.; Gilton, T. L.; Meier, W.; Cowin, J. P. *J. Chem. Phys*. **1990,** *92*, 2004.
(7) Marsh, E. P.; Schneider, M. R.; Gilton, T. L.; Tabares, F. L.; Meier, W.; Cowin, J. P. *Phys. Rev. Lett*. **1988**, *60*, 2551.
(8) Lu, P. H.; Lasky, P. J.; Yang, Q. Y.; Osgood, Jr., R. M. *Chem. Phys*. **1996**, *205*, 143.
(9) Holbert, V. P.; Garrett, S. J.; Stair, P. C.; Weitz, E. *Surf. Sci.* **1996**, *346*, 189.
(10) Howard, D.; Briggman, K. A.; Stair, P. C.; Weitz, E. *J. Chem. Phys.* **1995**, *102*, 7267.
(11) Bourdon, E. B. D.; Cowin, J. P.; Harrison, I.; Polanyi, J. C.; Segner, J.; Stanners, C. D.; Young, P. A. *J. Phys. Chem.* **1984**, *88*, 6100.
(12) Ramsier, R. D.; Yates, Jr., J. T. *Surf. Sci. Rep.* **1991**, *12*, 343.
(13) Ukraintsev, V.; Long, T. J.; Harrison, I. *J. Chem. Phys.* **1992**, *96*, 3957.
(14) Bourdon, E. B. D.; Das, P.; Harrison, I.; Polanyi, J. C.; Segner, J.; Stanners, C. D.; Williams, R. J.; Young, P. A. *Faraday Discuss. Chem. Soc.* **1986**, *82*, 343.
(15) Harrison, I.; Polanyi, J. C.; Young, P. A. *J. Chem. Phys.* **1988**, *89*, 1475.
(16) Lasky, P. J.; Lu, P. H.; Yang, M. X.; Osgood, Jr., R. M.; Bent, B. E.; Stevens, P. A. *Surf. Sci.* **1995**, *336*, 140.
(17) Yang, Q. Y.; Osgood, Jr., R. M. *J. Phys. Chem.* **1993**, *97*, 8855.
(18) Porret, D.; Goodeve, C. F. *Proc. R. Soc. London, Ser. A* **1938**, *165*, 31.
(19) Kimura, K.; Nagakura, S. *Spectrochim. Acta* **1961**, *17*, 166.
(20) Christodoulides, A. A.; Christophorou, L. G. *J. Chem. Phys.* **1971**, *54*, 11.
(21) Christophorou, L. G.; Carter, J. G.; Collins, P. M.; Christodoulides, A. A. *J. Chem. Phys.* **1971**, *54*, 11.
(22) Calvert, J. C.; Pitts, Jr., J. N. In *Photochemistry*; Wiley: New York, 1966.
(23) Black, S.; Lu, P. H.; Osgood, Jr., R. M.; Freisner, R. Accepted for publication in *Surf. Sci*.
(24) Liberman, V.; Nooney, M. G.; Amata, R. J.; Martin, R. M. *J. Phys. Chem*. **1993**, *97*, 2262.
(25) Lu, P. H.; Lasky, P. J.; Yang, Q. Y.; Wang, Y.; Osgood, Jr., R. M. *J. Chem. Phys.* **1994**, *101*, 11.
(26) Meyer, R. J.; Duke, C. B.; Paton, A.; Kahn, A.; So, E.; Yeh, J. L.; Mark, P. *Phys. Rev. B* **1979**, *19*, 10.
(27) *Advanced Series in Physical Chemistry Laser Spectroscopy and Photochemistry on Metal Surfaces Part II*; Dai, H. L., Ho, W., Eds.; World Scientific: Singapore, 1995; Vol. 5.
(28) Lasky, P. J.; Lu, P. H.; Khan, K. A.; Slater, D. A.; Osgood, Jr., R. M. To be published in *J. Chem. Phys.*
(29) Schwarz, W. N. Ph.D. Dissertation, Columbia University, 1992.
(30) Liberman, V. Ph.D. Dissertation, Columbia University, 1991.
(31) Berko, A.; Solymosi, F. *J. Phys. Chem.* **1989**, *93*, 12.
(32) Berko, A.; Erley, W.; Sander, D. *J. Chem. Phys.* **1990**, *93*, 8300.
(33) Zhou, X. L.; Solymosi, F.; Blass, P. M.; Cannon, K. C.; White, J. M. *Surf. Sci.* **1989**, *219*, 294.
(34) Zhou, X. L.; White, J. M. *Surf. Sci.* **1988**, *194*, 438.
(35) Henderson, M. A.; Mitchell, G. E.; White, J. M. *Surf. Sci. Lett.* **1987,** *187*, L325.
(36) Chen, J. G.; Beebe, Jr., T. P.; Cromwell, J. E.; Yates, Jr., J. T. *J. Am. Chem. Soc.* **1987,** *109*, 1726.
(37) Nuzzo, R. G.; Dubois, L. H. *J. Am. Chem. Soc.* **1986**, *108*, 2881.
(38) Albano, E. V. *Appl. Surf. Sci.* **1982**, *14*, 183.
(39) Albano, E. V. *J. Chem. Phys.* **1986**, *85*, 1044.
(40) Chan, C. M.; Aris, R.; Weinberg, W. H. *Appl. Surf. Sci*. **1978** *1*, 360.
(41) Falconer, J. L.; Schwarz, J. A. *Catal. Rev.—Sci. Eng*. **1983**, *25*, 141.
(42) Van Veen, G. N. A.; Baller, T.; De Vries, A. E. *Chem. Phys.* **1985**, *92*, 59.
(43) Redhead, P. A. *Vacuum* **1962**, *12*, 203.
(44) Costello, S. A.; Roop, B.; Liu, Z. M.; White, J. M. *J. Phys. Chem.* **1988**, *92*, 1019.
(45) Lloyd, K. G.; Roop, B.; Campion, A.; White, J. M. *Surf. Sci.* **1989**, *214*, 227.
(46) Zhou, X. L.; White, J. M. *Surf. Sci.* **1991**, *241*, 244.
(47) Modelli, A.; Scagnolari, F.; Distefano, G.; Jones, D.; Guerra, M. *J. Chem. Phys.* **1992**, *96*, 2061.
(48) Pearl, D. M.; Burrow, P. D. *J. Chem. Phys.* **1994**, *101*, 2940.
(49) Gerber, A.; Herzenberg, A. *Phys. Rev.* **1985**, *31*, 6219. Teillet-Billy, D.; Djamo, V.; Gauyacq, J. P. *Surf. Sci.* **1992**, *269/270*, 425. Rous, P. J. *Surf. Sci.* **1992**, *260*, 361.
(50) Vach, H.; Haeger, J.; Walther, H. *J. Chem. Phys.* **1989**, *90*, 6701. Rettner, C. T.; Schweitzer, E. K.; Mullins, C. B. *J. Chem. Phys.* **1989**, *90*, 3800.
(51) Comsa, G.; David, R. *Surf. Sci. Rep.* **1985**, *5*, 145.
(52) Anger, G.; Winkler, A.; Rendulic, K. D. *Surf. Sci.* **1989**, *220*, 1.
(53) Zhu, Q.; Cao, J. R.; Wen, Y.; Zhang, J.; Zhong, X.; Huang, Y.; Fang, W.; Wu, X. *Chem. Phys. Lett*. **1988**, *144*, 486.
(54) Kawasaki, M.; Kasatani, K.; Sato, H. *Chem. Phys.* **1984**, *88*, 135—142.
(55) Riley, S. J.; Wilson, K. R. *Faraday Discuss. Chem. Soc.* **1972**, *53*, 132.
(56) Herschbach, D. R. *Adv. Chem. Phys*. **1966**, *10*, 319.
(57) Zhou, X. L.; White, J. M. *Surf. Sci.* **1991**, *241*, 259.
(58) Zhou, X. L.; White, J. M. *Surf. Sci.* **1991**, *241*, 270.
(59) Banse, B. A.; Creighton, J. R. *Surf. Sci.* **1991,** *257*, 221.
(60) Garrett, S. J.; Heyd, D. V.; Polanyi, J. C. Submitted for publication in *J. Chem. Phys*.
(61) Swarm beam studies by Christophorou and co-workers[20,21] found that the dissociative electron attachment (DEA) cross section for ethyl bromide was peaked at an electron energy of only 0.76 eV while more recent studies put this value at 0.65 eV.[47] Note that these values are lower than the maximum in the electron attachment cross section (1.26 eV); this difference is indicative of the inability of DEA to compete with the increasing rate of autodetachment as the electron energy is increased.[48]